

# A Chemical Route to Graphene for Device Applications

Scott Gilje,<sup>†</sup> Song Han,<sup>‡</sup> Minsheng Wang,<sup>‡</sup> Kang L. Wang,<sup>‡</sup> and Richard B. Kaner<sup>\*†</sup>

*Department of Chemistry and Biochemistry and California NanoSystems Institute, University of California, Los Angeles, Los Angeles, California, 90095, and Department of Electrical Engineering and California NanoSystems Institute, University of California, Los Angeles, Los Angeles, California, 90095*

Received July 20, 2007; Revised Manuscript Received September 25, 2007

## ABSTRACT

Oxidation of graphite produces graphite oxide, which is dispersible in water as individual platelets. After deposition onto Si/SiO<sub>2</sub> substrates, chemical reduction produces graphene sheets. Electrical conductivity measurements indicate a 10000-fold increase in conductivity after chemical reduction to graphene. Tapping mode atomic force microscopy measurements show one to two layer graphene steps. Electrodes patterned onto a reduced graphite oxide film demonstrate a field effect response when the gate voltage is varied from +15 to -15 V. Temperature-dependent conductivity indicates that the graphene-like sheets exhibit semiconducting behavior.

Graphene is the name given to individual sheets of sp<sup>2</sup>-hybridized carbon bound in two dimensions of which crystalline graphite, the most thermodynamically stable form of carbon, is composed. Even though several other forms of sp<sup>2</sup> carbon including buckminsterfullerene (C<sub>60</sub>) and carbon nanotubes have been prepared, isolated, and studied during the past 2 decades, single-layer graphene has only recently been examined.<sup>1</sup> Over the past 2 years, a great deal of attention has been generated by graphene due to its unique electrical properties stemming from its semimetallic nature, which has produced properties such as the quantum Hall effect,<sup>2–5</sup> ambipolar electric field effect,<sup>1</sup> and transport via relativistic Dirac fermions.<sup>6,7</sup> More recently there have been attempts to observe the theoretical phenomenon known as the Klein paradox.<sup>8</sup> In addition to its fundamental electronic characteristics, graphene has been used to fabricate a number of simple electronic devices.<sup>9,10</sup> Graphene has also been used as reinforcement in polymer composites as it should be a less expensive substitute for carbon nanotubes.<sup>11</sup>

One of the driving forces in nanotechnology is to develop integrated circuits at a smaller scale than that possible with current silicon-based CMOS technology.<sup>12,13</sup> As silicon integrated circuits approach their theoretical limits, many researchers have turned to non-silicon-based materials in the

hope of discovering new materials upon which the next generation of electronic devices will be based.<sup>14,15</sup> Since graphene can exhibit room-temperature ballistic transport over mean free paths of up to 300 nm,<sup>16</sup> it has been suggested either as a channel material for the next generation of FETs or as a conductive sheet upon which nanometer scale devices may be patterned to create single electron or few electron transistors.<sup>16</sup> These attributes coupled with its nanometer scale, make graphene an excellent candidate for ultra-high-frequency transistors.<sup>17,18</sup>

At first glance it seems rather unusual that a detailed investigation of graphene would be so late in coming since graphite and its intercalation compounds have been studied for over 150 years. Then one realizes that graphene must be pulled from a monolith of highly oriented pyrolytic graphite (HOPG) by drawing as intercalation/exfoliation methods have failed to produce materials much below 100 nm<sup>19,20</sup> and the tools to effectively examine nanometer scale structures have only recently become widely available. By depositing peeled layers of graphite onto a 300 nm Si/SiO<sub>2</sub> substrate, Novoselov et al. were able to distinguish individual graphene layers using an optical microscope.<sup>1,16</sup> This provided a method to search the myriad of multilayered graphitic fragments left behind after drawing in order to find a single layer of graphene; a search that would have been nearly impossible using atomic force microscopy (AFM) alone. After a possible single sheet was located, AFM was used for verification. Although the technique of drawing has been improved somewhat by gently pushing graphene against a

\* Corresponding author. Telephone: (310) 825-5346. Fax: (310) 206-4038. E-mail: kaner@chem.ucla.edu.

<sup>†</sup> Department of Chemistry and Biochemistry and California NanoSystems Institute.

<sup>‡</sup> Department of Electrical Engineering and California NanoSystems Institute.

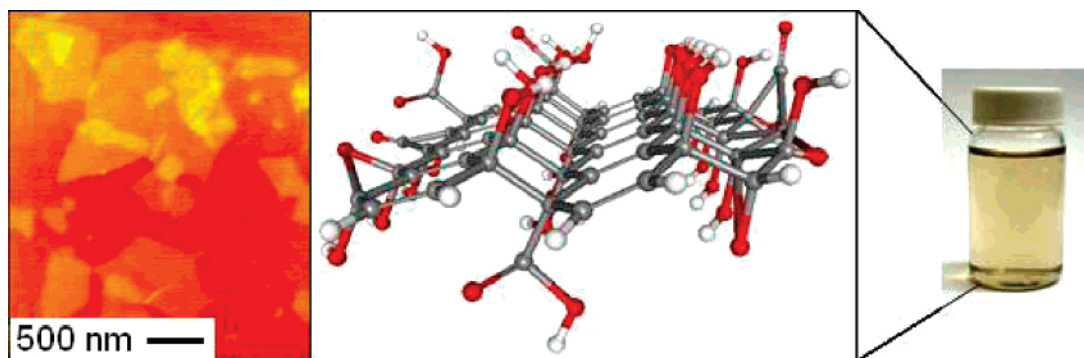


**Figure 1.** (a) An AFM image of GO platelets after deposition onto a Si wafer with a 300 nm SiO<sub>2</sub> epitaxial coating. (b) A three-dimensional molecular model of graphite oxide (GO) showing a puckered carbon sheet with –OH and –COOH functional groups (carbon = gray, oxygen = red, hydrogen = white). (c) A GO dispersion in water.

hard surface, it remains laborious and rudimentary in nature taking up to a week or more to locate a suitable specimen for making measurements.<sup>3,21,22</sup> Most of the reports on the electrical properties of graphene still use this method of peeling layers from HOPG using sticky tape and drawing onto a SiO<sub>2</sub> substrate in order to obtain graphene. More recently, some researchers have attempted to create large scale graphene using the reduction of SiC to form a single carbon layer through the loss of Si.<sup>14,23,24</sup> The size domains and uniformity of these films remain an issue. Additionally, the SiC synthesis requires a temperature in excess of 1100 °C, likely making this synthetic method costly should it be scaled up industrially. Hence, there exists a great need for an inexpensive, scalable method for achieving single-layer graphene.

Here we outline a process for preparing single and few layer graphene-like films exhibiting comparable electrical characteristics to bilayer graphene produced using the more time-consuming peeling/drawing method. This new method proceeds by way of a graphite oxide precursor as a means of achieving individual layers from bulk graphite. Graphite oxide has been known since 1860 when Brodie obtained it by treating graphite powder with a mixture of nitric acid and potassium nitrate.<sup>25</sup> In our experiments, graphite oxide is synthesized from graphite powder by a modified Hummers method as originally presented by Kovtyukhova et al.<sup>26,27</sup> Since graphite oxide (GO) is water dispersible due to the presence of oxygen-containing groups including carboxylic acid and hydroxyl moieties, it readily exfoliates upon sonication in water.<sup>26,28–30</sup> The structure of GO according to a recently proposed model by Dékány et al. is depicted in Figure 1b.<sup>28</sup> It is worth noting that this model is a refinement of an earlier model proposed by Scholz and Boehm, which is characterized by the lack of ether oxygens and the presence of corrugated carbon layers linked by ribbons exhibiting a quinoidal structure.<sup>31</sup> The presence of these functional groups on the GO surface leads to the enhanced interaction of GO with water. Figure 1c shows a vial containing a GO dispersion similar to the ones used for spray deposition.

After a good aqueous dispersion was achieved, the GO was deposited onto SiO<sub>2</sub> substrates. The deposition was originally attempted using standard drop-casting and dip-

coating techniques. However, these initial experiments all resulted in agglomeration of the GO platelets as the droplets of water evaporated and grew smaller. Since GO favors interactions with water over the SiO<sub>2</sub> substrate, the platelets remained dispersed in the water and simply became more concentrated as evaporation proceeded resulting in non-uniform films. Another set of experiments was then carried out using mixtures of water with nonaqueous solvents including dimethylformamide, methanol, ethanol, and acetone. In concentrations suitable for deposition (25–50 mg/L), the GO formed a stable dispersion in all of these solvents even in ratios as high as 19:1 parts solvent to water. Although use of a solvent mixture for drop-casting did facilitate the deposition of GO by reducing the degree of the resulting agglomeration, the films were still not uniform enough to carry out electrical measurements. In order to achieve a highly uniform deposition, our next approach involved spray depositing the GO dispersion onto a preheated substrate. In this way the GO platelets freeze upon contact with the substrate as the solvent flash evaporates. This technique combines small droplet size with rapid evaporation to avoid the concentration process that takes place upon slow solvent loss. AFM images of spray-deposited GO sheets are shown in Figure 1a. The sheets cover an area ranging from a few hundred nanometers up to 2 μm. Additionally, modulating the dispersion concentration and spray duration allows for precise control over the density with which the GO sheets are deposited. Coverage densities consisting of only a few independent sheets all the way up to continuous films of overlapping sheets can be obtained using this method. The spray deposition is highly uniform across the substrate showing the same coverage density across the sample. When electrodes were later patterned onto the deposited films, the yield of successful devices was nearly 100%.

Once the SiO<sub>2</sub> surfaces are spray-coated, the GO can be reduced chemically using hydrazine.<sup>32–34</sup> This was first attempted in open air by suspending the spray-coated substrate over anhydrous hydrazine heated to 80 °C. This heating both promotes vaporization and hastens the reduction reaction brought on by the hydrazine. However, this simple reduction setup causes hydrazine liquid, along with water

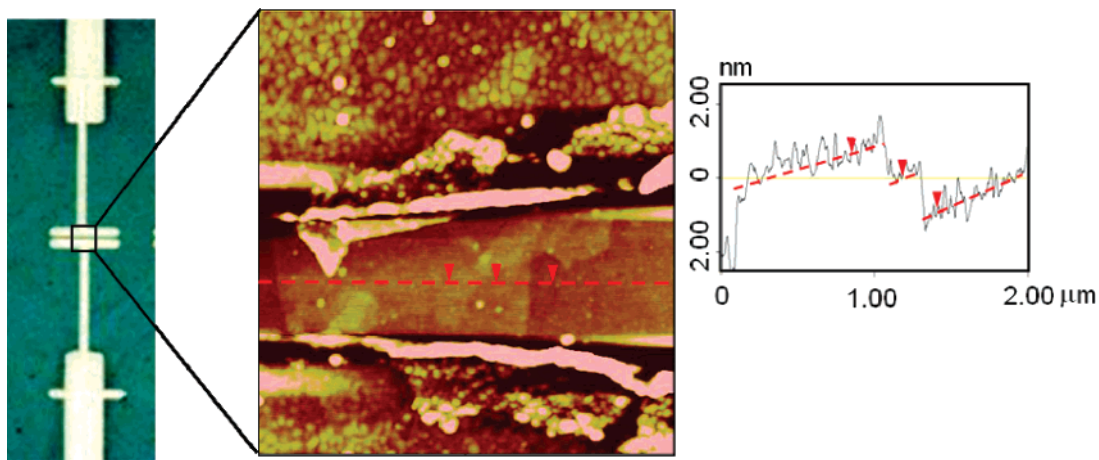


**Figure 2.** (a) Au electrodes are deposited by electron beam lithography on top of chemically reduced graphene oxide to form a transistor as imaged by an optical microscope. (b) The graphene sheets appear as thin platelets between the somewhat grainy gold electrodes as imaged by AFM. (c) When the AFM tip in tapping mode is moved across the graphene surface (red dotted line in b) steps of 8–9 Å are observed (red arrows).

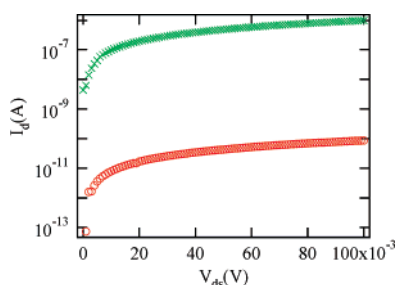


**Figure 3.** Current ( $I_d$ )–voltage ( $V_{ds}$ ) plots taken on graphite oxide films before (O) and after (x) reduction reveal a 10000-fold decrease in sheet resistance.

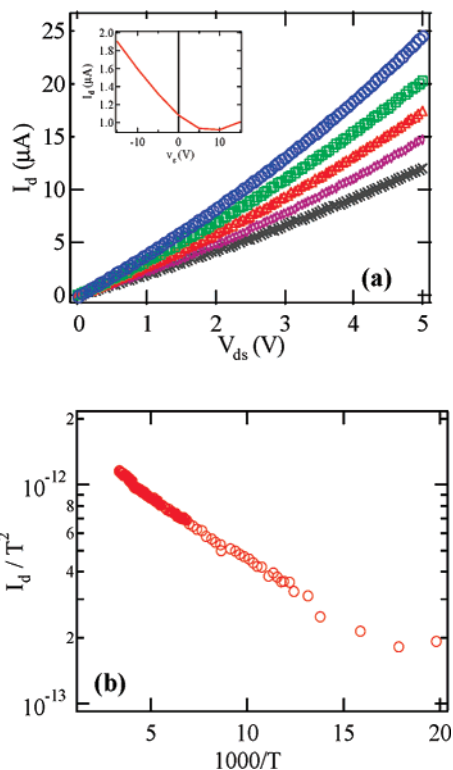
vapor drawn from the air to condense onto the substrates. This leads to agglomeration of the GO platelets during the reduction resulting in nonuniform films. To prevent condensation of water and hydrazine vapor, a flow cell was constructed so that the Si/SiO<sub>2</sub> substrate could be heated to 80 °C under a flow of helium gas with hydrazine vapor supplied via a bubbler.

Figure 2 shows an AFM image of an as-fabricated device with a few sheets of reduced graphene oxide film between the two electrodes. The cross-sectional height profile shows that the thickness of the graphite oxide film is 0.8–0.9 nm, a height consistent with two layers of graphene. In order to obtain electrical measurements of the films, GO was deposited in a sufficient density to form a continuous film of overlapping platelets. Figure 2 shows optical microscopy and AFM images of the electrodes as-deposited on the graphene film. Since only graphite oxide films bridge from the source to the drain electrodes, the measured resistivity should indicate if the deposition and reduction was successful.

The first electrical test is a comparison of the conductivity difference between the graphite oxide and reduced graphene films. In Figure 3, the measured sheet resistance of the graphite oxide film is  $\sim 4 \times 10^{10} \Omega$  per square, while the reduced graphite oxide is  $\sim 4 \times 10^6 \Omega$  per square. To confirm

that the change of conductance is due to graphite oxide reduction, over 100 devices were measured before and after the vapor-phase reduction reaction. The conductance was observed to increase by a factor of  $10^4$ – $10^5$  in almost every device. A representative example of one of the devices tested is depicted in Figure 2. The conductivity increases upon exposure to hydrazine due to deoxygenation of graphite oxide to create C–C and C=C bonds. Although this reaction is unlikely to result in a perfect graphene structure, enough carbon double bonds are established to create conducting pathways leading to the resulting increase in the observed conductivity.<sup>32</sup> The deoxygenation of GO to produce a conducting material can also be confirmed through the use of Raman spectroscopy. In their recent work, Stankovich et al. noted a distinct change in the Raman spectrum going from GO to reduced GO after exposure to hydrazine.<sup>35</sup> The results of our Raman measurements agree with those of Stankovich lending evidence that the GO has been at least partially deoxygenated.

Our next set of experiments tested the field effect responses of the reduced graphene oxide films. The measurements were carried out in air at room temperature using the same global back-gated FET devices. The tests used a Si substrate as the back gate. While the gate bias was varied from –15 to +15 V, the resistance of the device increased from 0.20 to 0.42 M $\Omega$  (see Figure 4a). The increase in conductivity as the voltage is lowered indicates that the reduced graphene oxide films are p-type semiconducting materials. The temperature dependence of the device’s resistance is presented in Figure 4b. The material shows semiconducting-type behavior; i.e., as the temperature decreases, the resistance of the reduced graphene film increases. The  $I/T^2$  versus inverse temperature ( $1/T$ ) data fits well to a Schottky contact model, which confirms a semiconductor/metal interface. As Figure 4b shows, the results fit a Schottky contact model which is formulated as  $I_d = AT^2 e^{-q(\Phi - V)/kT}$ . Therefore, by plotting  $I_d/T^2$  versus  $1/T$ , we can get the Schottky barrier height  $\Phi =$



**Figure 4.** (a) Current ( $I_d$ )–voltage ( $V_{ds}$ ) of reduced graphite oxide film devices. As the gate voltage changes from +15 to –15 V, the conductance of the device increases, indicative of a p-type semiconductor. The curves from bottom to top correspond to the gate bias of 15, 0, –5, –10, and –15 V, respectively. The inset shows the  $I$ – $V_g$  curve at  $V_{ds} = 0.5$  V. (b) Temperature-dependent measurements confirm that reduced graphene films exhibit semiconducting behavior—decreased conductance at lower temperatures.

54.8 meV. This lends further evidence that the reduced graphite oxide films act as semiconductors.

Graphite can be chemically oxidized to make graphite oxide which disperses in water forming a colloidal suspension of graphite oxide (GO) sheets. Through the addition of –OH and –COOH groups by chemical oxidation, the  $\pi$  system of the parent graphite has been disrupted. This in turn reduces the van der Waals forces holding the graphene sheets together and enables them to be dispersed upon sonication in water. Thin layers of GO can be deposited onto SiO<sub>2</sub> substrates preheated to 150 °C. Varying the concentration and the spray duration of the GO dispersion allows precise control over the coverage density of sheets deposited onto the substrate. Once deposited, the GO can be reduced using hydrazine vapor, which acts to deoxygenate the GO and reestablish carbon–carbon double bonds. This process produces a measured resistance change of 4–5 orders of magnitude. Further testing reveals that the reduced graphene acts as a p-type semiconductor and exhibits a field effect response.

This spraying method can be used to obtain graphene sheets of any desired coverage density with great uniformity and nearly 100% yield. Since the graphene-like sheets are sprayed at 150 °C, this process can be scaled to deposit sheets onto a number of substrates, of any size, and even onto

prepatterned electrodes with great confidence, thus minimizing the need for characterization while improving throughput. Unlike current syntheses that use SiC as a starting material, high temperatures (i.e., 1100 °C or greater) are not required. Additionally, our spray-coating method is quick, taking only a few hours to yield sheets. This marks a significant advantage over current mechanical methods that have a very low yield of randomly distributed individual graphene sheets, requiring a period of at least a week to search for a suitable graphene specimen. For these reasons we believe our spraying method has the potential for the large scale deposition of graphene for use in electronic devices.

**Acknowledgment.** This work has been supported by the Focused Center Research Program’s Functional Engineered Nano Architectonics Center (FENA/FCRP) and the Air Force Office of Scientific Research (AFOSR). We thank Christina Baker for help acquiring TEM images.

**Supporting Information Available:** Descriptions of graphite oxide synthesis, GO spray coating and reduction, electrode fabrication, and electrical property measurements. This material is available free of charge via the Internet at <http://pubs.acs.org>.

## References

- Novoselov K. S.; Geim A. K.; Morozov S. V.; Jiang D.; Zhang Y.; Dubonos S. V.; Grigorieva I. V.; Firsov A. A. *Science* **2004**, *306* (5696), 666–9.
- Gusynin V. P.; Sharapov S. G. *Phys. Rev. Lett.* **2005**, *95* (14), 146801.
- Zhang, Y.; Tan, Y.W.; Stormer, H. L.; Kim, P. *Nature* **2005**, *438* (7065), 201–204.
- Novoselov, K. S.; McCann, E.; Morozov, S. V.; Fal’ko, V. I.; Katsnelson, M. I.; Zeitler, U.; Jiang, D.; Schedin, F.; Geim, A. K. *Nat. Phys.* **2006**, *2* (3), 177–180.
- Novoselov, K. S.; Jiang, Z.; Zhang, Y.; Morozov, S. V.; Stormer, H. L.; Zeitler, U.; Maan, J. C.; Boebinger, G. S.; Kim, P.; Geim, A. K. *Science* **2007**, *315* (5817), 1379.
- Novoselov, K. S.; Geim, A. K.; Morozov, S. V.; Jiang, D.; Katsnelson, M. I.; Grigorieva, I. V.; Dubonos, S. V.; Firsov, A. A. *Nature* **2005**, *438* (7065), 197–200.
- Zhou, S. Y.; Gweon, G. H.; Graf, J.; Fedorov, A. V.; Spataru, C. D.; Diehl, R. D.; Kopelevich, Y.; Lee, D. H.; Louie, S. G.; Lanzara, A. *Nat. Phys.* **2006**, *2* (9), 595–599.
- Katsnelson, M. I.; Novoselov, K. S.; Geim, A. K. *Nat. Phys.* **2006**, *2* (9), 620–625.
- Bunch J. S.; van der Zande A. M.; Verbridge S. S.; Frank I. W.; Tanenbaum D. M.; Parpia J. M.; Craighead H. G.; McEuen P. L. *Science* **2007**, *315* (5811), 490–3.
- Staley, N.; Wang, H.; Puls, C.; Forster, J.; Jackson, T. N.; McCarthy, K.; Clouser, B.; Liu, Y. *Appl. Phys. Lett.* **2007**, *90* (14), 143518/1–143518/3.
- Stankovich, S.; Dikin, D. A.; Dommett, G. H. B.; Kohlhaas, K. M.; Zimney, E. J.; Stach, E. A.; Piner, R. D.; Nguyen, S. T.; Ruoff, R. S. *Nature* **2006**, *442* (7100), 282–286.
- Gargini, P. Sailing with the ITRS into Nanotechnology. Presentation at Semicon west July 12, 2004.
- 2007 International Technology Roadmap for Semiconductors.
- Berger, C.; Song, Z.; Li, T.; Li, X.; Ogbazghi, A. Y.; Feng, R.; Dai, Z.; Marchenkov, A. N.; Conrad, E. H.; First, P. N.; de Heer, W. A. *J. Phys. Chem. B* **2004**, *108* (52), 9912–19916.
- Hass, J.; Feng, R.; Li, T.; Li, X.; Zong, Z.; de Heer, W. A.; First, P. N.; Conrad, E. H.; Jeffrey, C. A.; Berger, C. *Appl. Phys. Lett.* **2006**, *89* (14), 143106/1–143106/3.
- Geim, A. K.; Novoselov, K. S. *Nat. Mater.* **2007**, *6* (3), 183–191.
- Brey, L.; Fertig, H. A. *Phys. Rev. B* **2006**, *73* (23), 235411/1–235411/5.
- Son, Y. W.; Cohen, M. L.; Louie S. G. *Phys. Rev. Lett.* **2006**, *97* (21), 216803.

- (19) Viculis, L. M.; Mack, J. J.; Kaner, R. B. *Science* **2003**, *299* (5611), 1361.
- (20) Shioyama, H.; Akita, T. *Carbon* **2003**, *41* (1), 179–181.
- (21) Novoselov, K. S.; Jiang, D.; Schedin, F.; Booth, T. J.; Khotkevich, V. V.; Morozov, S. V.; Geim, A. K. *Proc. Natl. Acad. Sci. U.S.A.* **2005**, *02* (30), 10451–10453.
- (22) Castro, A.; Guinea, F.; Peres, N. M. *Phys. World* **2007**, 33–37
- (23) Berger, C.; Song, Z.; Li, X.; Wu, X.; Brown, N.; Naud, C.; Mayou, D.; Li, T.; Hass, J.; Marchenkov, A. N.; Conrad, E. H.; First, P. N.; de Heer, W. A. *Science* **2006**, *312* (5777), 1191–1196.
- (24) Ohta, T.; Bostwick, A.; Seyller, T.; Horn, K.; Rotenberg, Eli. *Science* **2006**, *313* (5789), 951–954.
- (25) Brodie, B. *Ann. Chim. Phys.* **1855**, *45*, 351.
- (26) Kovtyukhova, N. I.; Ollivier, P. J.; Martin, B. R.; Mallouk, T. E.; Chizhik, S. A.; Buzaneva, E. V.; Gorchinskiy, A. D. *Chem. Mater.* **1999**, *11* (3), 771–778.
- (27) Hummers, W. S., Jr.; Offeman, R. E. *J. Am. Chem. Soc.* **1958**, *80*, 1339.
- (28) Lerf, A.; He, H.; Forster, M.; Klinowski, J. *J. Phys. Chem. B* **1998**, *102* (23), 4477–4482.
- (29) Szabo, T.; Berkesi, O.; Forgo, P.; Josepovits, K.; Sanakis, Y.; Petridis, D.; Dékány, I. *Chem. Mater.* **2006**, *18* (11), 2740–2749.
- (30) Lerf, A.; Buchsteiner, A.; Pieper, J.; Schoettl, S.; Dékány, I.; Szabo, T.; Boehm, H. P. *J. Phys. Chem. Solids* **2006**, *67* (5–6), 1106–1110.
- (31) Scholz, W.; Boehm, H. P. *Z. Anorg. Allg. Chem.* **1969**, *369* (3–6), 327–340.
- (32) Stankovich, Sasha; Piner, Richard D.; Chen, Xinqi; Wu, Nianqiang; Nguyen, S. T.; Ruoff, Rodney S. *J. Mater. Chem* **2006**, *16* (2), 55–158.
- (33) Liu, P.; Gong, K. *Carbon* **1999**, *37* (4), 706–707.
- (34) Bourlinos, A. B.; Gournis, D.; Petridis, D.; Szabo, T.; Szeri, A.; Dékány, I. *Langmuir* **2003**, *19* (15), 6050–6055.
- (35) Stankovich, Sasha; Dikin, Dmitriy A.; Piner, Richard D.; Kohlhaas, Kevin A.; Kleinhammes, Alfred; Jia, Yuanyuan; Wu, Yue; Nguyen, SonBinh T.; Ruoff, Rodney S. *Carbon* **2007**, *45* (7), 1558–1565.

NL0717715